International Journal of Heat and Mass Transfer 226 (2024) 125467

Contents lists available at ScienceDirect

International Journal of Heat and Mass Transfer

journal homepage: www.elsevier.com/locate/ijhmt

Heating efficiency of agarose samples doped with magnetic nanoparticles subjected to ultrasonic and magnetic field

Barbara Gambin *, Eleonora Kruglenko, Ryszard Tymkiewicz, Jerzy Litniewski

Institute of Fundamental Technological Research, Polish Academy of Sciences, Department of Ultrasound, ul. Pawinskiego 5B, 02-106 Warsaw, Poland

ARTICLE INFO

Keywords:
Magnetic nanoparticle-mediated hyperthermia
Dual-mode ultrasonic-magnetic hyperthermia
Specific absorption rate
Hyperthermia efficiency

ABSTRACT

Recently, magneto-ultrasound heating of tissue in the presence of magnetic nanoparticles (NPs) has been studied due to its high potential for use in oncological hyperthermia. It has been published that a synergistic effect, generation of additional heat caused by magneto-ultrasonic coupling, was observed in a tissue-mimicking material (TMM) enriched with magnetic NPs. The specific absorption rate (SAR) was determined from the temperature rise measurements in a focus of the ultrasound beam. It is important to use precise measurement methods when considering medical applications, for which there are limitations to the power of each field, resulting from the prevention of biological phenomena dangerous to the patient. This study demonstrates that in magneto-ultrasonic heating SAR can be measured much more accurately if the ultrasonic field is almost uniform. Measurements were performed on TMM containing Fe_3O_4 NPs with a diameter of approximately 8 nm and superparamagnetic properties. Both, the measurement and simulation results showed that the errors resulting from the inaccuracy of placing the temperature probe are smaller than in the case of the focused ultrasound. At the same time, the temperature increase caused by the ultrasonic field is almost linear and the influence of heat convection on the SAR determination is negligible. The measurements showed that magneto-ultrasonic hyperthermia can provide the desired thermal effect at lower ultrasound powers and magnetic fields compared to ultrasonic or magnetic hyperthermia used alone. No synergy effect was recorded.

1. Introduction

Multimodal therapies, especially those combining hyperthermia with chemo- therapy and radiotherapy, are currently at the center of research on modern minimally invasive cancer therapies, cf. [1]. Bi-modal therapy combining magnetic nanoparticles (NPs) mediated magnetic hyperthermia and radiotherapy are discussed in the paper [2]. The selection of the type and size of magnetic nanoparticles added to cancer tissue was optimized due to two parameters: the effectiveness of magnetic hyperthermia and radiotherapy measured by the specific absorption rate (SAR) and by the dose enhancement factor (DEF), respectively. Ultrasonic-magnetic hyperthermia using magnetic nanoparticles is an interesting alternative to tissue heating methods. Studies of such dual-mode hyperthermia are of practical importance, as they can limit the intensity of each of the independently operating fields, ultrasonic and magnetic. At the same time, they try to answer the question of whether the interaction of coupled magnetic and ultrasonic fields on magnetic nanoparticles can lead to measurable additional thermal effects.

Quantum effects must be considered to explain the thermal processes in materials in the presence of nanoparticles. In particular, the quantum effect is responsible for the appearance of a photon layer on the surface of the nanoparticle from which the ultrasonic wave is reflected [3]. This effect results in increased heat production in samples containing crystalline iron oxide nanoparticles during ultrasonic hyperthermia, cf. [4], [5]. The influence of the addition of nanoparticles to the Si/Ge superlattice on the reduction of thermal conductivity was investigated [6]. In turn, [7] describes the influence of the size and shape of nanoparticles on increasing the thermal conductivity of argon-based nanoliquids. Under the influence of a changing electromagnetic or mechanical field (in particular ultrasounds), the active processes of heat transport in nano liquids change, see [8]. Numerical modeling of the effect of doping tissues with nanoparticles and generating heat under the influence of ultrasound (ultrasonic hyperthermia) is still the subject of intensive research, e.g. in [9], the influence of the porous tissue structure enriched with nanoparticles on the temperature distribution in the tumor during HIFU treatment was investigated.

* Corresponding author.
E-mail address: bgambin@ippt.pan.pl (B. Gambin).

https://doi.org/10.1016/j.ijheatmasstransfer.2024.125467
Received 30 August 2023; Received in revised form 12 March 2024; Accepted 19 March 2024

The effect of the simultaneous action of ultrasonic and magnetic fields in two-mode hyperthermia, proposed in [10] and [11] was experimentally studied using different samples of ferrofluid and ferrogel. In the research, studies using agar-based ferrogel are of particular interest because agar gel is the basis of tissue phantoms used in ultrasound examinations as a material mimicking soft tissue. Doping the agar gel phantoms with magnetic iron oxide nanoparticles increases the absorption of ultrasonic waves, but the properties of the phantom remain in the range of soft tissue properties [5] and [12].

The properties of ferrogels have been intensively studied due to their application in magnetic field-assisted drug delivery, positioning, and biosensing see [13] and [14]. Regardless of biomedical applications, the study of soft gels controlled by a magnetic field was discussed in the review [15] in terms of their high-impact potential applications in soft robotics/devices and metamaterials. The wide application of magnetic hydrogels also included applications in devices related to environmental applications such as environmental remediation see [16]. Much less research has been devoted to the study of ferrogels using ultrasounds.

The group of authors of papers [14] and [17] studied the use of ultrasound imaging of samples of chemical magnetic hydrogel with a PPA (Polyphthalamide) matrix with different content of iron oxide nanoparticles with a size of 100 nm. The effect of the NPs concentration in the gel on the elasticity and acoustic impedance was investigated.

The influence of nanoparticles on the gel polymerization process (including the degree of hardness) is strongly dependent on whether the gel is physical or chemical, as well as on other parameters influencing the polymerization structure. The elastic susceptibility of the ferrogel was tested by an ultrasonic recording of the ferrogel deformation under the influence of a variable magnetic field acting on the nanoparticles fixed inside the gel. Such measurements were used to assess the hardness of tissues containing magnetic nanoparticles [18] and [19]. The influence of magnetic nanoparticles in gels on structural changes under the influence of ultrasounds has not been sufficiently studied. The hypothesis is that the addition of magnetic nanoparticles with a size of approx. 100 nm to the gel results in higher absorption of ultrasounds than the addition of non-magnetic nanoparticles has been discussed and initially confirmed experimentally see [5] and [4] and [20].

Meanwhile, the question of the existence of a coupling (synergy) between the action of ultrasonic waves and an alternating magnetic field in the phenomenon of converting mechanical (ultrasound) and electromagnetic energy into heat on magnetic nanoparticles remains open. To prove this, one would have to show that ultrasound absorption increases in an alternating magnetic field and/or vice versa and that magnetic absorption increases under the influence of ultrasound.

The authors of [11] in the dual-mode hyperthermia studies stated the hypothesis that they can detect the effect of coupling between magnetic and ultrasonic fields when ultrasound and magnetic field act simultaneously on ferrogel samples. In the conducted tests, the temperature measurement was recorded at points close to the focus of the ultrasonic beam. However, the result of the presented measurements is difficult to interpret. Both the nature of the temperature rise curves and the range of changes, especially in the initial phase, are significantly different when the sample is heated with a magnetic field and an ultrasonic field. This makes it difficult to compare them with each other and makes it difficult to assess the contribution of both fields, working together or separately, to the ferrogel heating efficiency.

Therefore, the issue of coupling interactions between the magnetic field and ultrasound and the possibility of measuring these coupling effects remains open. To prove such effects and results to be reliable, measurements should be made several times, each time in a new sample and a new placement of the temperature probe in the sample. Such operations undoubtedly cause differences in the position of the sample and the probe in subsequent measurements. It can be assumed that the magnetic field is uniform in the ferrogel sample and, consequently, the magnetic field evenly heats the sample throughout its volume. Therefore, inaccuracies in the position of the probe measuring the temperature caused by the magnetic field have a negligible effect on the temperature increase curves determined for subsequent samples. Also, heat convection is small and therefore has little effect on the rate of increase of the measured temperature. It looks completely different when the sample is heated with a focused ultrasonic field. The probe is placed in the focus area, i.e. in the area of large temperature gradients. Small differences in the position of the probe relative to the focus have a large impact on the result of temperature measurement in subsequent samples. In addition, when measuring the temperature in the first seconds of heating with a probe placed in the focus, due to large spatial temperature gradients, heat convection has a large influence on the measured temperature rise curve.

In this research, a measurement was carried out in a sample placed in a homogeneous ultrasonic field is proposed. This should significantly reduce the errors in temperature estimation compared to measurements in the focus, errors resulting from the low repeatability of the probe position. The measurement performed in a homogeneous ultrasonic field also allows for a significant reduction in the impact of the convection phenomenon. As a result, the nature of the temperature increase curve should be similar to the curve obtained when heating with a magnetic field, which will increase the accuracy of comparing the contributions of both fields to the temperature increase. The presented research will demonstrate that the value of the SAR coefficient (Specific Absorption Rate), which is a commonly used measure of heating efficiency, determined from the temperature rise curve during heating using both fields, is the sum of the SAR coefficients measured separately for the ultrasonic field and the magnetic field.

Additionally, by modeling the ultrasonic field in the sample, the temperature differences in the sample resulting from the distribution of the ultrasonic field amplitude will be estimated for two cases: the sample located outside the focus of the ultrasonic transducer and in the focus.

2. Materials and methods

Ferrogel samples with properties similar to soft tissue (acoustic attenuation, sound speed, density) were prepared for the study of ultrasonic-magnetic hyperthermia (UMHT). Two heat sources of different natures, an alternating magnetic field, and an ultrasonic field were generated by a generator with a coil and an ultrasonic transducer. The tested sample was placed in a container with water to enable the transmission of ultrasounds and to stabilize the ambient temperature of the sample. The temperature in the sample was recorded with an optical thermometer, first under the influence of only ultrasounds, then only the magnetic field, and finally under the influence of both fields acting simultaneously. Numerical modeling was performed in COMSOL Multiphysics and MATLAB programs.

2.1. Preparation of agarose-based samples with Fe_3O_4 nanoparticles

Fe_3O_4 nanoparticles coated with PEG (Polyethylene Glycol) were synthesized by chemical co-precipitation. An aqueous solution containing ferrous (Fe^{2+})/ferric (Fe^{3+}) ions and PEG-400 (Avantor (POCH)) was prepared. Ammonium hydroxide (NH4OH) was used to precipitate the nanoparticles. Then, the nanoparticles were purified using ethanol and acetone and dried in a vacuum oven. A detailed description of the procedure can be found in [21].

The composition of the nanoparticles was determined based on the analysis of the FTIR (Fourier Transform Infrared) spectrum, performed using the Perkin Elmer FTIR-ATR 100 instrument (MA, USA). The size of nanoparticles was determined from images obtained from transmission microscope (TEM) JEOL 1011 (USA) and X-ray diffraction (XRD) measurements using diffractometer D8 Discover (Bruker, Germany), see [21] and [22].

FTIR analysis confirmed that the obtained nanoparticles consist of Fe_3O_4 and a PEG layer. Magnetic hysteresis was measured for the pro-

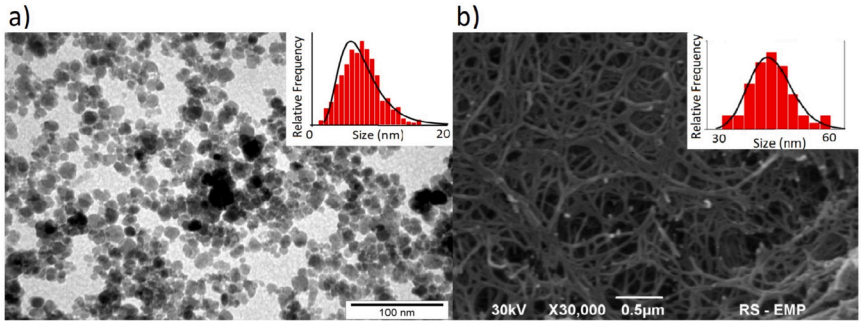

Fig. 1. a) Transmission electron microscope image of PEG-coated Fe_3O_4 nanoparticles. The histogram of the nanoparticle size distribution is additionally placed at the top of the figure. b) Scanning electron microscope images of an agar-based sample containing nanoparticles. Additionally, a histogram of the thickness distribution of agar fibers is placed at the top of the figure.

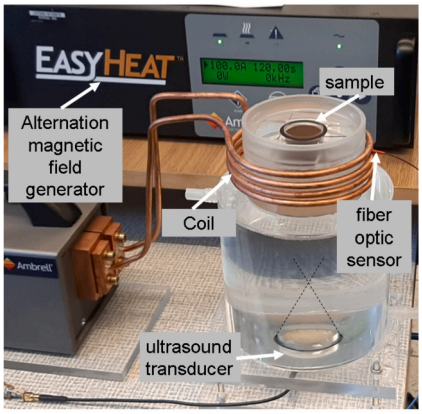

Fig. 2. Experimental setup for magnetic-ultrasonic hyperthermia.

duced nanoparticles, which confirmed their superparamagnetic properties, see [21] and [22]. The size of the nanoparticles determined from the TEM images was 7.6 ± 2.7 nm, and derived from the Shererr formula using diffraction peak analysis (in XRD) was 8.9 ± 1.02 nm. The fabricated tissue mimic material (TMM), ferrogel, contained 2% agarose (Agarose Broad Range, Carl Roth) with Fe_3O_4 coated with PEG at a concentration of 40 mg/mL aqueous agarose, see Fig. 1.

The mixture was sonicated in an ultrasonic bath (Sonorex DT 52H, Bandelin Electronics, Germany) for 8 hours at 80 °C to obtain a uniform distribution of the nanoparticles and to prevent their deposition. After the mixture was cooled ton55 °C, the contents were poured into plexiglass cylinders 28 mm in diameter and 25 mm long, 10 samples were produced to avoid repeated thermal measurements on the same sample.

The parameters of the agar sample with nanoparticles were determined experimentally. In the simulations, the ultrasonic attenuation coefficient was assumed to be 0.24 dB/MHz cm, speed of sound = 1494 m/s, specific heat = 4177 J/(kg K), and thermal conductivity = 0.55 W/m K.

2.2. Experimental setup

The system consisted of two water containers made of plexiglass, a smaller one at the top and a larger one at the bottom (Fig. 2).

The larger container had a diameter of 140 mm and a height of 120 mm, and the smaller container had a diameter of 90 mm and a height of 60 mm. A smaller container was placed inside a coil that produced an alternating magnetic field. A cylinder-shaped sample with a diameter of 26 mm and a height of 20 mm was placed in a smaller container, symmetrically to the axis of the ultrasonic beam, at a distance of 150 mm from the spherical, focusing ultrasonic transducer, which was placed at the bottom of the larger container.

With this arrangement, the alternating magnetic field produced by the coil did not affect the ultrasonic transmitter. The water layer served both to transmit ultrasound and to isolate the sample from the heat generated during operation by the ultrasonic transducer and the magnetic coil. An ultrasonic heating transducer with a resonant frequency of 2.5 MHz, a focal length of 60 mm, and an acoustic power of 7 W, generating a signal of 1000 periods, repeated every 1.6 ms, duty cycle of 0.4, was used to generate the ultrasonic field. The acoustic power of the ultrasonic transducer was measured with a radiation force balance (Ultrasound Power Meter, Ohmic Instruments Co., USA). The generator (Agilent Technologies 33250A, USA) and RF amplifier (ENI.INC Model 3100LA, USA) were used to transmit ultrasonic signals.

The temperature was measured using an optical thermometer, and the thermometer's sensor was located in the center of the sample at a distance of 160 mm from the surface of the transducer (100 mm from the focus of the beam). A fiber optic thermometer FOTEMP1-H with a TS3 temperature sensor (OPTOCON, Germany) with a resolution of 0.1 °C and a response time of 250 ms was used. The sensor was placed perpendicularly to the symmetry axis of the ultrasonic transmitting beam.

An EASYHEAT kit (Ambrell Cooperation, USA) with a four-turn coil was used to generate the alternating magnetic field. The frequency of the magnetic field was set to 250 kHz. Magnetic field strength H on the axis of symmetry of the coil/solenoid was calculated according to Biot-Savart low by the following formula [23]:

$$H(z) = \frac{NI}{2L}\left(\frac{-z+\frac{L}{2}}{\sqrt{\left(-z+\frac{L}{2}\right)^2+R^2}} + \frac{z+\frac{L}{2}}{\sqrt{\left(z+\frac{L}{2}\right)^2+R^2}},\right) \quad (1)$$

where N is the number of turns, I is the electric current intensity, L is the length of the solenoid, R is the solenoid radius and z is the distance from the center of the solenoid to the point on the axis where the magnetic field strength is calculated. The magnetic field inside the sample of ferrogel located in the central part of the soil was nearly spatially homogeneous, cf [24]. For the experimental conditions $N = 4$, $R = 50$ mm, $L = 40$ mm and $I = 50\ kA$. The maximum magnetic field strength was in the center of the coil and it was equal to $H(0) = 1.85\ kA/m$.

The main goal was to investigate the process of temperature increase changes in dual hyperthermia, in which both "heating" fields have heat sources almost evenly distributed in the sample volume and the temperature increases in the initial seconds when heated with each field separately are qualitatively similar. The selected parameters of the measurement system ensured that these conditions were met and at the same time were within the limits clinically accepfor hyperthermia therapy.

2.3. Specific absorption rate (SAR)

An important parameter characterizing the efficiency of hyperthermia is the specific absorption rate, SAR measured in [W/kg] (or equivalently, SLP-specific loss power). Determining the SAR from the calorimetric experimental data requires knowledge of the temperature rise curve in the sample. The SAR is defined as follows [20]

$$SAR = C_p \left(\frac{dT}{dt}\right)_{t=0} \tag{2}$$

where C_p, [J/(kg·K)] denotes the specific heat of sample, $\left(\frac{dT}{dt}\right)_{t=0}$ is a measured initial slope of the heating curve (in the case of a continuum, the value of the derivative of the curve at the initial time).

It is assumed that the SAR in UMHT can be determined in the physical model of heat transfer, in which there are three types of heat sources: ultrasound heat, magnetic field heat, and heat from the mutual action (coupling) of both of these fields:

$$\rho SAR = Q^{acoustic} + Q^{magnetic} + Q^{synergy}, \tag{3}$$

where ρ denotes the density of the TMM with magnetic nanoparticles, $Q^{acoustic}$, $Q^{magnetic}$, $Q^{synergy}$ are the heat sources caused by ultrasound and magnetic fields separately, and by the heat generation due to coupling/interaction between both fields acting simultaneously, respectively. From eq. (3) it follows:

$$\rho SAR = \rho SAR^{acoustic} + \rho SAR^{magnetic} + Q^{synergy}, \tag{4}$$

and finally:

$$\left(\frac{dT}{dt}\right)_{t=0,UMHT} - \left(\frac{dT}{dt}\right)_{t=0,UHT} - \left(\frac{dT}{dt}\right)_{t=0,MHT} = \left(\frac{Q^{synergy}}{\rho C_p}\right). \tag{5}$$

The subscripts in the above expressions refer to UMHT - ultrasonic magnetic hyperthermia, UHT - ultrasonic hyperthermia, and MHT - magnetic hyperthermia respectively. The numerical determination of the SAR coefficient in dual ultrasonic-magnetic hyperthermia requires knowledge of the theoretical values of the coupling component, i.e. a description of the physical coupling of the sound field and the magnetic field for magnetic nanoparticles, which is currently unknown. Therefore, one can only look for the existence of synergy, i.e. the non-zero value of the right-hand side in the eq. (5), by determining the sum of the derivatives at zero from the curves of temperature increase in ultrasonic, magnetic, and dual ultrasonic-magnetic hyperthermia.

The SAR value, i.e. the rate of temperature increase, depends on many parameters such as the physical properties of both fields and the material properties of the medium on which these fields act. Therefore, determining the conditions under which SAR reaches its maximum value as a function of one or more parameters simultaneously remains a challenge for science. Research has been carried out to find the maximum SAR value in the case of exposure to magnetic field only. Due to biosafety restrictions on the density of nanoparticles and their chemical composition, performance control was based on the selection of the intensity and frequency of the field. e.g. [25–27]. No analogous considerations have been found in the literature when SAR is associated with both fields operating simultaneously.

The experimental values of the derivatives at the zero of the temperature rise curves were estimated by approximating the temperature rise curves with the linear function $T(t) = at$. The measurement curves used to determine the SAR were obtained by averaging the results of 10 measurements of heating the samples successively by the ultrasonic field, the alternating magnetic field, and both fields acting together. The temperature rise curves were recorded over 3 minutes. For each type of heating, average values of temperature increase and standard deviations were calculated.

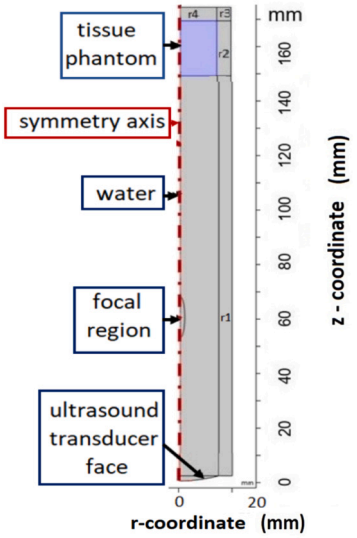

Fig. 3. Geometric model of the computational area made in COMSOL. Half of the cross-section of the considered axially symmetric problem is presented in a cylindrical system with coordinates (r, z). At the top, the location of the soft tissue sample is marked in blue, and then the area covered by water is marked in gray, in which the location of the ultrasound beam focusing field is marked. r1, r2, r3 and r4 at the edges of the calculation area denote damping layers for ultrasonic waves. A cross-section of the ultrasonic transducer is marked on the lower edge. The axis of symmetry of the system is marked with a red dashed line.

2.4. Numerical model of ultrasound field distribution and heating

The numerical model makes it possible to determine the space-time distribution of the temperature field caused by ultrasound. The numerical model was necessary to evaluate the spatial changes of the temperature field inside the tissue (sample). Neither the measurement of the sound pressure, which determines the amount of heat released in the sample, nor the reliable measurement of the temperature distribution can be carried out inside the samples. Temperature measurements with an optical thermometer were made only at one point inside the sample, and the measurement of the sound pressure distribution generated by the ultrasonic transducer was made in water.

To calculate the space-time temperature distribution caused by the ultrasonic field, the COMSOL Multiphysics 4.3b program was used, which combines the problems of ultrasonic wave propagation and heat exchange in a sonicated medium. The numerical model consists of two connected modules. In the first one, the spatial distribution of the acoustic field (pressure) in the sonicated area is determined, in this case inside the tested TMM sample. In the second module, the spatial temperature distribution during ultrasound operation is determined using the equation for Bioheat Transfer. A detailed description of how the modules work can be found in the work [20].

The geometry of the task, shown schematically in Fig. 3, is a representation of the experimental set-up intended for testing the temperature increase in the sample under the action of an ultrasonic beam. The ultrasound is focused below the sample location as shown in Fig. 2. Both the sample and the acoustic transducer are submerged in a water tank and arranged coaxially, and the transducer is circular, hence the model was defined as axisymmetric, 2D.

During the calculations (simulation) the constant temperature at the edges of the sample (T = 20 °C) was assumed equal to the initial temperature of the sample and the environment. For comparison, temperature distribution simulations were also carried out assuming no heat flow at the edges of the sample.

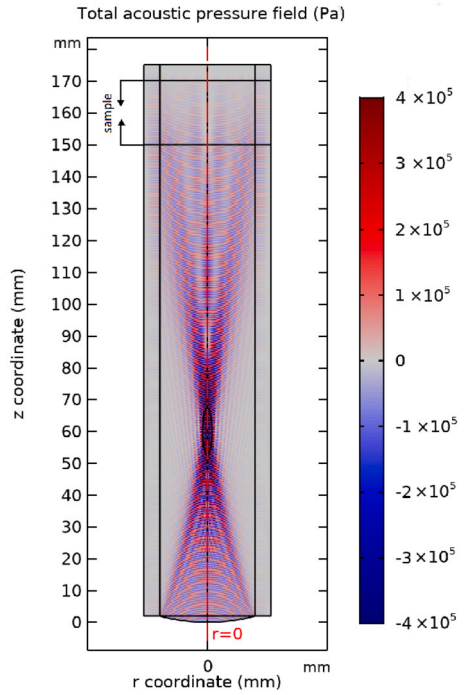

Fig. 4. Distribution of the acoustic pressure field (in pascals, Pa) emitted by the focusing ultrasonic transducer, calculations in Comsol. Cross-section along the ultrasonic beam. The lower edge of the image shows a cross-section of the front of the ultrasonic transducer. The position of the sample is marked at a distance of 100 mm behind the focus.

3. Results and discussion

3.1. Validation of the numerical model

Numerical simulation made it possible to determine the pressure of the acoustic wave in both liquid tanks and in the sample placed 100 mm from the focus, see Fig. 4. The distribution of sound pressure was calculated for the measuring system, schematically shown in Fig. 3.

Validation of the numerical model was carried out by comparing the experimental results with the prediction of the model. Namely, the shape of the acoustic field in water was measured, perpendicular to the direction of ultrasonic beam propagation, in the focus of the beam and outside the focus. Measurements were made with a hydrophone, (0.2 mm, Needle Hydrophone PA). The voltage measured with a hydrophone in [mV] was converted into sound pressure in [MPa] following the information provided by the manufacturer of the hydrophone. The sound pressure of 1 MPa corresponded to a voltage of 549.4 mV at a frequency of 2.5 MHz.

Fig. 5 shows the results obtained at a distance of 150 mm from the transducer. The curves of the measured and calculated pressures have similar values and shapes, which allows for a positive assessment of numerical predictions.

Fig. 6 shows the pressure values measured with a hydrophone and the values calculated from the numerical model both in the vicinity of the focus of the ultrasonic transducer and in the area 100 mm behind the focus (160 mm from the transducer), i.e. in the area proposed for SAR determination.

Again, the pressure distributions, measured and calculated, are very similar. The obtained results were also used to assess the temperature measurement error resulting from the accuracy of the location of the temperature sensor in subsequent measurements.

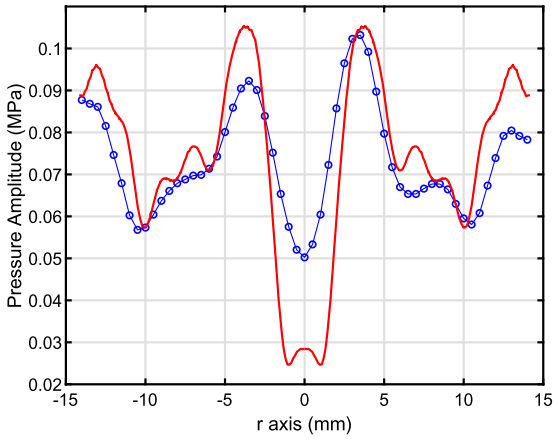

Fig. 5. Sound pressure distribution in water (cross-section perpendicular to the beam direction) at a distance of 100 mm behind the transducer focus. Hydrophone measurement result - blue curve and simulation result - red curve.

3.2. Numerical results of ultrasound field distribution and heating

In the next step, simulations of temperature distribution inside the sample heated for 30 seconds with ultrasound were carried out. Fig. 7 presents distributions of temperature changes at a distance of up to 15 mm from the ultrasound beam axis for two cases, in the focus area (depth 50-70 mm) and outside the focus (depth 150-170 mm).

The temperature difference between the focus and 1 mm from the focus is about 20.4 °C. If the sample is placed 100 mm from the focus, the difference in temperature at the axis of the beam and 1 mm from the axis is only about 0.04 °C.

An assessment of the impact of boundary conditions on temperature changes during ultrasonic heating was also carried out when measuring the temperature with an optical sensor with an accuracy of 0.1 °C. Two cases were simulated in a sample placed outside the focus, a case of constant temperature at the edge equal to the initial temperature of the sample and no heat flow at the sample boundary. The results of the simulation are shown in Fig. 8. After 30 s of heating, the differences in temperature increase at points 1 mm away from the center of the sample were about 0.03 °C, which is much less than the accuracy of the temperature sensor.

In addition, Fig. 9 shows the numerically calculated increase in temperature during heating of the sample for two cases, when the transducer is focused in the sample and the temperature is measured at the focus, and for the second case when the temperature is measured in the center of the sample located 100 mm behind the focus. It can be seen that for the location of the sample away from the focus, the relationship between the temperature and the time of heating the sample with ultrasound is almost linear.

3.3. Experimental results for magnetic heating

Fig. 10 shows the results of temperature rise measurements in TMM samples placed in an alternating magnetic field and the average values from these measurements with marked standard deviations.

3.4. Results for combined ultrasonic-magnetic heating and SAR approximation

Fig. 11 presents the results of temperature measurements for 30 s and 180 s for three heating methods: ultrasonic - UHT, magnetic - MHT, and magnetic-ultrasonic - UMHT. Measurements were carried out for 10 samples.

Fig. 12 presents the average temperature values measured over 60 seconds for 10 samples during three heating methods (UHT, MHT and

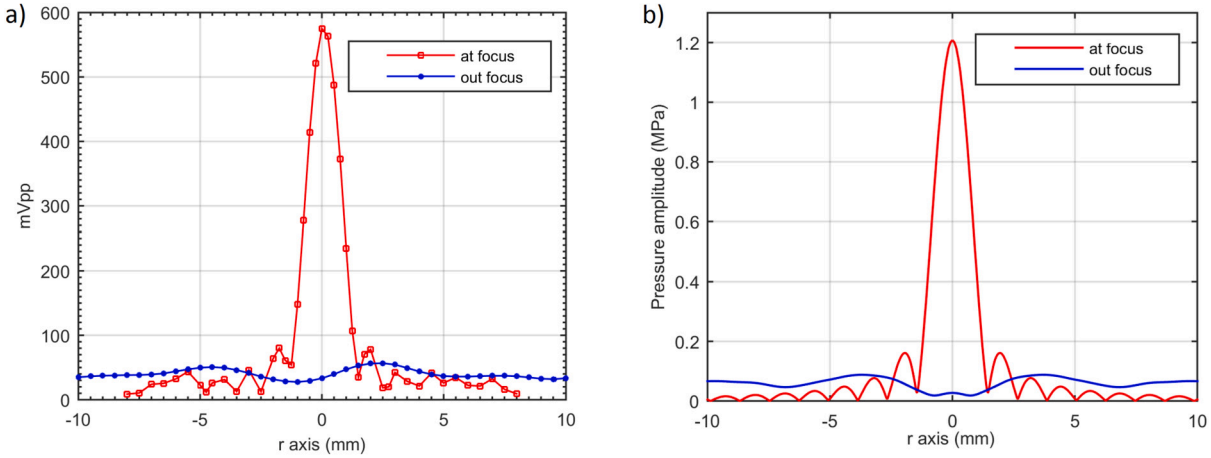

Fig. 6. Cross-section of the pressure distribution generated by the transducer in water, a) measured with a hydrophone, and b) simulated in Comsol. The red curve indicates the distribution at the transducer's focus and the blue curve indicates the distribution 100 mm behind the focus.

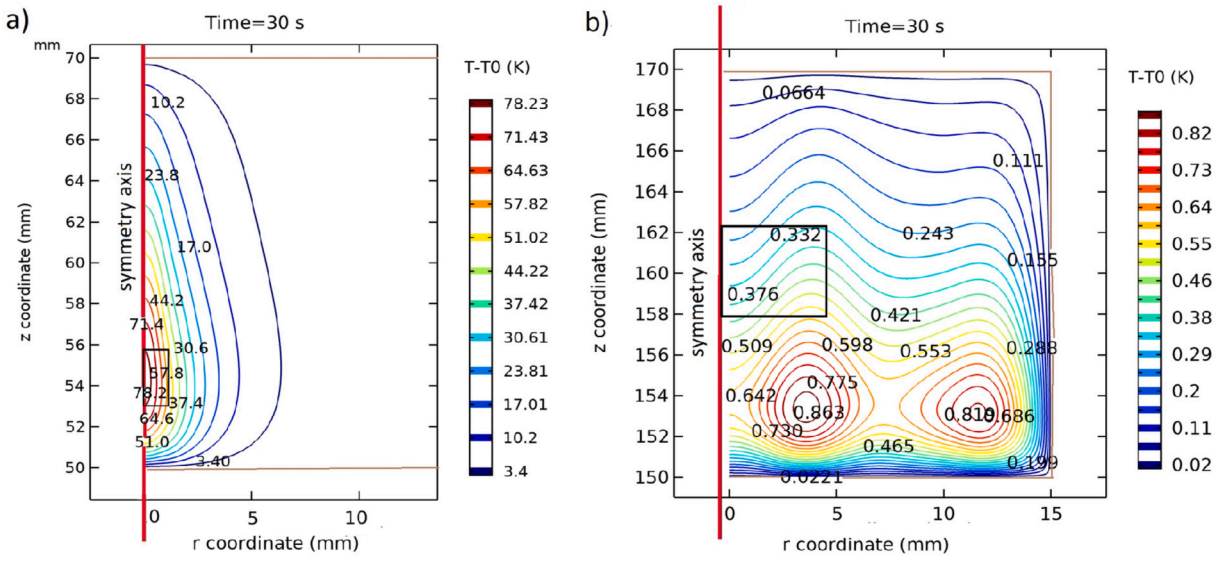

Fig. 7. Maps of isothermal temperature rise lines (in Kelvin, K) calculated after 30 seconds of sonication. a) sample placed at the focus, and b) 100 mm behind the focus. In figure a), a 1x2 mm square indicates the location of the focus, and in figure b), a 4x4 mm square marks the area in the center of which the temperature probe was placed.

UMHT) and the result of summing the temperature measurement curves for UHT heating and MHT heating.

Determining the SAR coefficient requires calculating the derivative of the temperature-time function at the initial moment of heating. For this purpose, experimental data describing the dependence of temperature on heating time were approximated by a linear function. The measure of the accuracy of fitting R^2 to the linear function in ultrasonic heating (UHT), magnetic heating (MHT), and ultrasonic-magnetic heating (UMHT) was 0.826, 0987, and 0.952, respectively.

Table 1 shows the average SAR values and standard deviations for experimental temperature rise data determined by fitting the rise curves to a linear function, taking into account data from the first 15 s, 30 s, and 100 s of heating. SAR values have been determined for ultrasonic, magnetic, and simultaneous ultrasonic and magnetic heating. Also presented are the corresponding values of the coefficients of variation (CV = mean/SD) and the sum of the SAR for UHT and MHT. Note that when calculating the SAR over a longer period of time, the SAR values decrease significantly for UHT and UMHT, a bit less for MHT. This is due to the non-linearity of the temperature increase in the first seconds of ultrasonic heating.

But at the same time, when the data collected from the longer time, from 15 s to 100 s, were used for SAR calculations, the accuracy of fitting R^2 to the linear function in ultrasonic heating (UHT), magnetic heating (MHT), and ultrasonic-magnetic heating (UMHT) increased from 0.826, 0987, and 0.952 to 0.991, 0.995, 0.991, respectively. Besides, the standard deviations strongly decreased. Also, in the case of collection time increased to 100 s, the coefficient of variations (CV) decreased significantly compared to 15 s collection time. Namely, in ultrasonic heating (UHT), magnetic heating (MHT), and ultrasonic-magnetic heating (UMHT) CV decreased from 0.42, 0.07, and 0.21 for data collected from 15 s to 0.09, 0.03, and 0.06 respectively, for data collected from 100 s, Table 1. It can be concluded that planning hyperthermia based on parameters determined on the basis of measurements of the temperature increase after 30 seconds of heating, and even more so after 100 seconds, is more reliable than using information from measurements after 15 seconds of heating. Additionally, the level of SAR dispersion in UMHT is at least twice lower than in UHT itself, which means that the use of bimodal hyperthermia reduces the error in determining the heating efficiency of tissue containing magnetic nanoparticles.

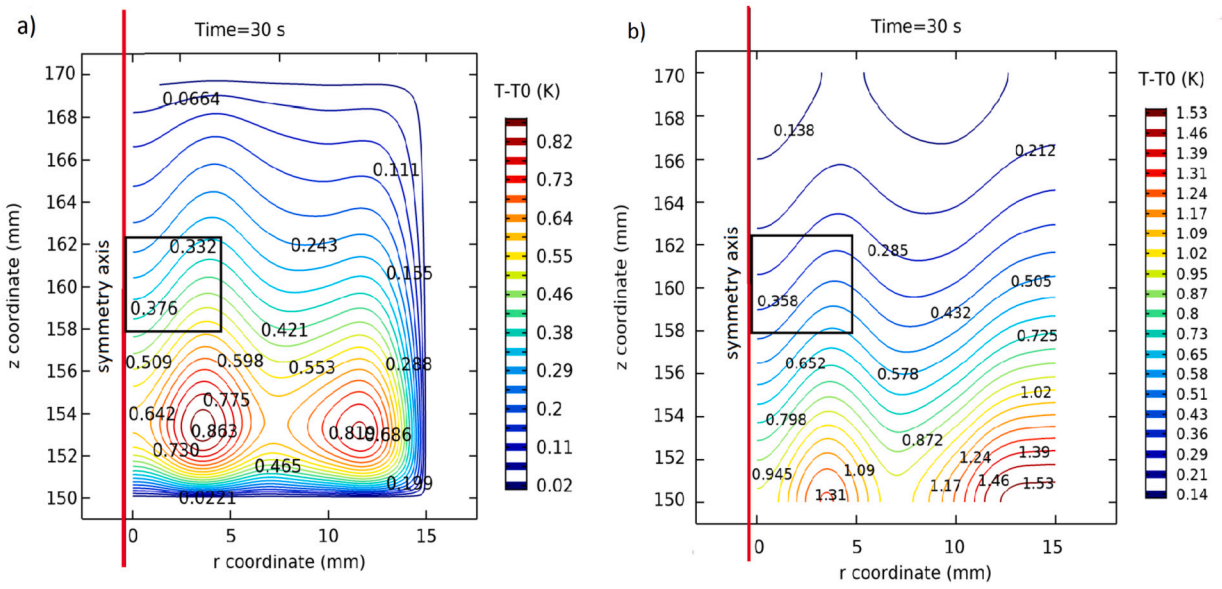

Fig. 8. Maps of isothermal lines of temperature increase (in Kelvin, K) calculated after 30 seconds of sonication of a sample placed 100 mm behind the focus. A 4x4 mm square marked the area in the center of which the temperature probe was placed. The boundary condition a) of constant temperature (20 °C) at the edges of the sample, and b) the condition of no heat flow at the edges of the sample were assumed in the calculations.

Table 1
Averaged SAR (W/kg) with SD - standard deviation, and CV - coefficient of variation, for three types of heating, and three data collections time intervals 15 s, 30 s and 100 s. UHT denotes ultrasonic heating, MHT - magnetic heating, UMHT - simultaneous ultrasonic and magnetic heating, UHT+MHT - the sum of the respective SAR values.

	Time 15 s			Time 30 s			Time 100 s		
Heating	SAR	SD	CV	SAR	SD	CV	SAR	SD	CV
UHT	186	79	0.42	138	44	0.31	97	9	0.09
MHT	249	18	0.07	243	9	0.04	234	3	0.03
UMHT	423	87	0.21	383	48	0.12	332	18	0.06
UHT+MHT	435			381			332		

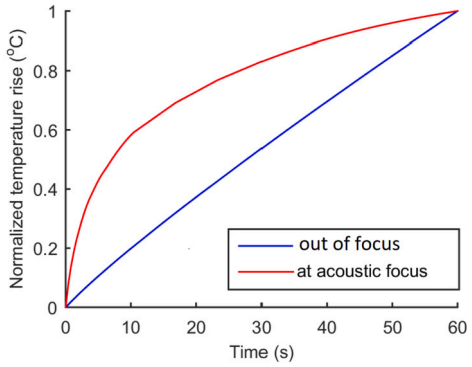

Fig. 9. Simulation of the temperature increase during 60 seconds measured in the center of the sample for the case of placing the sample at the transducer focus (red curve) and for placing the sample 100 mm behind the focus, in an almost uniform ultrasonic field (blue curve). Curves normalized to the maximum value.

The evaluation of the numerical model confirmed the compliance of the spatial pressure distributions with the distributions determined numerically and measured experimentally, cf. e.g. [28], as well as compliance with the measurement made at the focus and 100 mm behind the focus. In measurements as well as in the calculations of the shape of the pressure profile across the beam far from the focus, there are diffraction effects in the form of two distinct maxima located on either side of the central axis of the beam, see Fig. 6. On this basis, it can be concluded that the simulations of the acoustic field inside the sample are also consistent with real sound pressure distributions that cannot be determined experimentally. Let us note that in the case of locating the beam focus inside the sample, the simulation of the acoustic field using the linear model of ultrasonic wave propagation is burdened with a large error due to the non-linear effects (thermal effect of generation of higher harmonics) being not taken into account in the simulation. Such effects are very limited when the sample is placed outside the focus, i.e. in an ultrasonic field with a lower intensity than in the focus.

It has been shown that the method of measuring temperature in a sample placed outside the focus of the ultrasonic beam, as compared to measurements in the focus, has several significant advantages. Firstly, such a measurement shows little sensitivity to the error of the position of the temperature probe. Secondly, the measurement shows a small influence of convection in the first seconds of heating on temperature changes, which entails an almost linear increase in temperature with heating time. The convection-related non-linearity of the temperature increase is proportional to the measure of the spatial non-uniformity of the sound pressure distribution inside the sample, i.e. non-zero temperature gradients. Since the linear temperature increase is also observed during spatially uniform heating with a variable magnetic field, as a result, determining the SAR from the observed temperature increase by estimating the linear function in UHT and UMHT is more reliable.

An additional advantage of the proposed procedure for measuring the temperature away from the focus is that the influence of the boundary conditions on the change in the temperature increase during the first

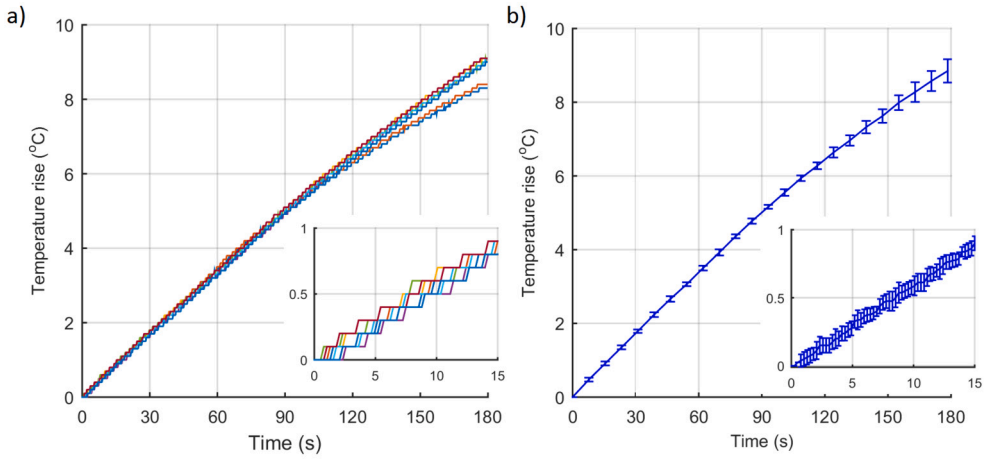

Fig. 10. Temperature increase in the sample measured while heating 10 samples with a magnetic field for 180 seconds. a) temperature increase curves in each of 10 samples, b) average value of 10 results with standard deviation (SD). Additionally, the results obtained during the first 15 seconds of heating are presented.

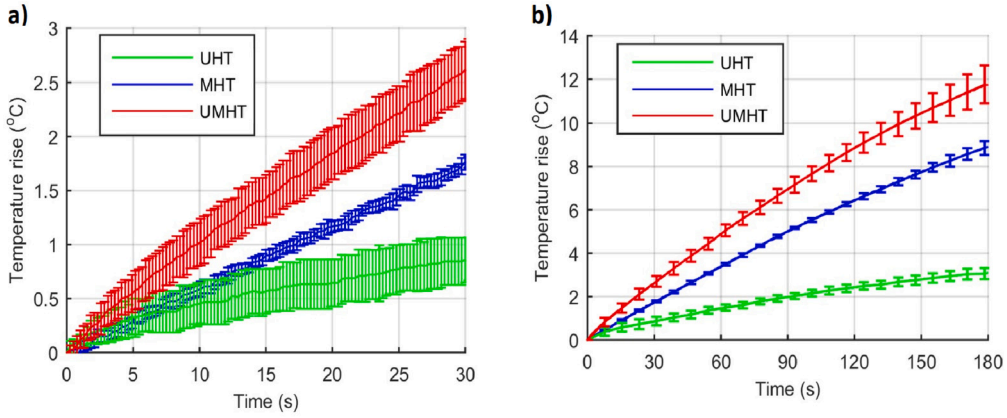

Fig. 11. Curves of temperature increase as a function of heating time using ultrasonic hyperthermia (UHT) - green, magnetic hyperthermia (MHT) - blue and coupled ultrasonic-magnetic hyperthermia (UMHT) - red. Each curve shows the average temperature value obtained from 10 samples along with standard deviations (SD). Results obtained during a) 30, and b) 180 seconds of heating.

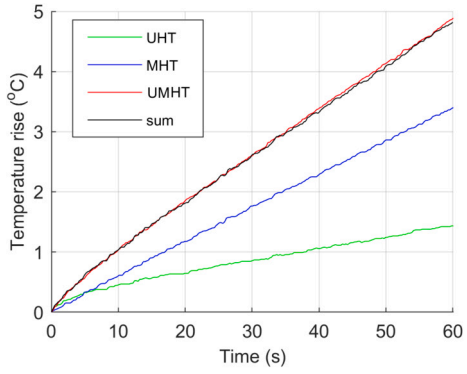

Fig. 12. Temperature increase versus heating time curves averaged from the results obtained for 10 samples using ultrasonic hyperthermia (UHT) - green, magnetic hyperthermia (MHT) - blue and coupled ultrasonic-magnetic hyperthermia (UMHT) - red. Additionally, the algebraic sum of the results obtained for ultrasonic and magnetic hyperthermia is marked with a black line. The curves for UMHT and those obtained from the summation coincide.

dozen or so seconds of heating is negligibly small, which was shown by the numerical simulation.

Note that in the experiments carried out in which the temperature rise curves were measured, it was not possible to ensure thermal insulation of the edges of the tested sample, but a constant temperature outside. Such thermal conditions simulate the conditions of hyperthermia in a living organism, in which the perfusion mechanisms strive to maintain a constant temperature. Thus, there is a constant temperature outside the tissue area containing the nanoparticles when subjected to hyperthermia fields. Of course, this causes a heat transfer from the heated area to the cooler outdoor area. For this reason, the measured temperature rise curve becomes curved after the first few tens of seconds. The numerical model was used to prove that this effect had little influence on the rate of temperature change in the initial seconds of the heating process, and thus on the SAR value.

Based on the obtained experimental results, it was found that in the range of temperature determination accuracy (0.1 °C), in the range of transmitting acoustic power up to 7 W, for an alternating magnetic field with an intensity of H= 1.85 kA/m and a frequency of f= 250 kHz, no acoustic-magnetic coupling caused by the existence of magnetic nanoparticles in a tissue-mimicking material, which would result in the generation of additional heat, was found.

Perhaps this phenomenon occurs when a magnetic field of higher intensity and/or frequency is used, or nanoparticles of larger size or magnetic susceptibility are used. The optimal size of magnetic nanoparticles in ferrofluid that maximizes SAR is approximately 15-20 nm [29], [30], when SAR is calculated assuming low magnetic field strengths. Larger nanoparticles cease to exhibit superparamagnetic properties. However, when forming aggregates, when NPs are located in the cellular environment (as is the case in cancer therapy), not only the size of the nanoparticles but also their mutual position and dipole and multi-field

interactions begin to play an important role [31]. Used in the study nanoparticles had a size of approximately 8-9 nm. The thickness of the PEG layer was estimated at approx. 1-2 nm. Certainly, enlarging the size of NPs can improve the magnetic heating performance, and changing the size of the PEG coating can change the amount of heat released during ultrasonic sonication of ferrogel. If the appearance of the synergy effect dependence on the size of the fields used is assumed, then if the heating efficiency of each type of heating (magnetic and ultrasonic) increases, the synergy effect could be measurable. Similarly, it is possible that high-intensity ultrasonic waves (such as those that appear at the focus of an ultrasonic beam) can weaken the bonds of the agar gel enough to alter the Brownian relaxation of nanoparticles in the medium. This thesis was formulated in [10], [11]. The research was conducted outside the focus when the intensity of the ultrasonic wave was relatively low but spatially homogeneous, and any additional effect that would indicate synergy, i.e. mutual interaction of both fields was observed.

Nanoparticles were coated with PEG. The question arises whether this can affect the change in the structure of the nanoparticle surface and, consequently, its interaction with the magnetic and ultrasonic fields. In the case of an ultrasonic wave, its length is so large compared to the size of the nanoparticle that the medium with nanoparticles can be considered a continuous medium, so the shape of the nanoparticles and, of course, the surface do not influence the wave. However, if the hypothesis of increased ultrasonic absorption as a result of the appearance of a special phonon layer on the nanoparticle surface is true in the case of doping the sample with nanoparticles, a PEG coating of the nanoparticle should be considered. Particle surface conditions can likely alter magnetic SAR. Assessment of the impact of changes in the surface structure of the Fe_3O_4 crystal, which were related to the existence of the PEG coating, was beyond the capabilities of this research.

The main limitation of the obtained results is the relatively low-intensity level of the acoustic fields causing the heating effect in the area of the sample where the temperature measurement is made. Also, the alternating magnetic field remained within a limited, biologically safe range, which does not lead to the excitation of large eddy currents in the tissue. The product of the alternating magnetic field frequency and its strength was $1.85\ \text{kA/m} \cdot 250\ \text{kHz} = 4.625 \cdot 10^8\ \text{A/m·s}$.

4. Conclusion

The proposed new method of determining SAR for ultrasonic heating, consisting in placing the TMM sample outside the focus of the ultrasonic transducer, in a homogeneous ultrasonic field, provides numerous advantages compared to the method of placing the sample in the focus of the ultrasonic beam. The simulations performed showed that, firstly, it significantly reduces the error resulting from differences in the position of the temperature sensor. At the same time, it greatly limits the impact of thermal boundary conditions and heat convection on the measurement result of the temperature rise curves from which SAR is determined. Both measurements and simulations also showed that when using a uniform ultrasonic field, the measured temperature increases almost linearly during heating, similar to the curve obtained with magnetic heating. Similar, linear increases in both temperature curves are important in experiments seeking synergy when heating with an ultrasonic and magnetic field. The measurement results when heating the TMM with an ultrasonic and magnetic field at biologically safe intensities allowed to obtain an increase in the temperature of the tested samples by 5 degrees (60 sec) or 12 degrees (120 sec). Raising the temperature of the tumor tissue to about 42 degrees supports oncological treatment - radiotherapy and immunotherapy or chemotherapy. This is the range of temperature increase required for oncological hyperthermia. Within this power range, it has been shown that the SAR calculated from the temperature rise of the sample when the two fields are operated simultaneously is equal to the sum of the SARs obtained from the temperature rise measurements when the fields are operated separately. It was found that by using magneto-ultrasonic hyperthermia, the desired thermal effect can be obtained at lower intensities of each field than when using magnetic or ultrasonic hyperthermia separately. This is important for the safety of hyperthermia therapy.

CRediT authorship contribution statement

Barbara Gambin: Writing – review & editing, Writing – original draft, Validation, Supervision, Methodology, Investigation, Formal analysis, Conceptualization. **Eleonora Kruglenko:** Visualization, Software, Data curation. **Ryszard Tymkiewicz:** Funding acquisition, Data curation. **Jerzy Litniewski:** Writing – review & editing, Supervision, Project administration, Conceptualization.

Declaration of competing interest

I, Barbara Gambin as the corresponding author of the paper ent. “Heating efficiency of agarose samples doped with magnetic nanoparticles subjected to ultrasonic and magnetic field”, declare on behalf of all the authors of the submission the lack of any financial and personal relationships with other people or organizations that could inappropriately influence (bias) our work.

Data availability

No data was used for the research described in the article.

Acknowledgement

We would like to thank Dr. Mateusz Zieliński and Prof. Piotr Koniorczyk from the Military University of Technology for measuring the thermal properties of ferrogel samples. We would like to express our special thanks to the anonymous reviewers whose accurate substantive comments made it possible to correct the deficiencies in the work.

One of the authors of this work (JL) was partially supported by grant no. 2019/35/B/ST7/03792 from the National Science Centre of Poland.

References

[1] S. Shirvalilou, Z. Tavangari, M.H. Parsaei, S. Sargazi, R. Sheervalilou, M. Shirvaliloo, H. Ghaznavi, S. Khoei, The future opportunities and remaining challenges in the application of nanoparticle-mediated hyperthermia combined with chemo-radiotherapy in cancer, WIREs Nanomed. Nanobiotechnol. 15 (6) (2023) e1922, https://doi.org/10.1002/wnan.1922.

[2] A.S. Davydov, A.V. Belousov, G.A. Krusanov, M.A. Kolyvanova, B.B. Kovalev, A.S. Komlev, P.V. Krivoshapkin, V.N. Morozov, V.I. Zverev, Promising magnetic nanoradiosensitizers for combination of tumor hyperthermia and X-ray therapy: theoretical calculation, J. Appl. Phys. 129 (3) (2021) 033902, https://doi.org/10.1063/5.0032843.

[3] S. Simons, On the interaction of long wavelength phonons with thermal phonons, Proc. Phys. Soc. 83 (5) (1964) 749, https://doi.org/10.1088/0370-1328/83/5/306.

[4] C. Bera, S.B. Devarakonda, V. Kumar, A.K. Ganguli, R.K. Banerjee, The mechanism of nanoparticle-mediated enhanced energy transfer during high-intensity focused ultrasound sonication, Phys. Chem. Chem. Phys. 19 (2017) 19075–19082, https://doi.org/10.1039/C7CP03542J.

[5] B. Gambin, E. Kruglenko, R. Tymkiewicz, J. Litniewski, Ultrasound assessment of the conversion of sound energy into heat in tissue phantoms enriched with magnetic micro- and nanoparticles, Med. Phys. 46 (10) (2019) 4361–4370, https://doi.org/10.1002/mp.13742.

[6] Y. Liu, Y. Li, K. Shen, Y. Qiu, J. Xie, Further decrease of the thermal conductivity of superlattice through embedding nanoparticle, Int. J. Heat Mass Transf. 203 (2023) 123789, https://doi.org/10.1016/j.ijheatmasstransfer.2022.123789.

[7] R. Zhang, X. Zhang, S. Qing, Z. Luo, Y. Liu, Investigation of nanoparticles shape that influence the thermal conductivity and viscosity in argon-based nanofluids: a molecular dynamics simulation, Int. J. Heat Mass Transf. 207 (2023) 124031, https://doi.org/10.1016/j.ijheatmasstransfer.2023.124031.

[8] Y. Ueki, Y. Yamamoto, T. Ohara, M. Shibahara, Molecular dynamics study of energy transport mechanism in nanofluids: spatial and component decompositions of effective thermal conductivity, Int. J. Heat Mass Transf. 202 (2023) 123746, https://doi.org/10.1016/j.ijheatmasstransfer.2022.123746.

[9] T. Wessapan, P. Rattanadecho, Flow and heat transfer through a porous tumor during high-intensity focused ultrasound, Int. J. Heat Mass Transf. 216 (2023) 124501, https://doi.org/10.1016/j.ijheatmasstransfer.2023.124501.

[10] K. Kaczmarek, T. Hornowski, I. Antal, M. Timko, A. Józefczak, Magneto-ultrasonic heating with nanoparticles, J. Magn. Magn. Mater. 474 (2019) 400–405, https://doi.org/10.1016/j.jmmm.2018.11.062.
[11] K. Kaczmarek, T. Hornowski, I. Antal, M. Rajnak, M. Timko, A. Józefczak, Sono-magnetic heating in tumor phantom, J. Magn. Magn. Mater. 500 (2020) 166396, https://doi.org/10.1016/j.jmmm.2020.166396.
[12] E. Kruglenko, M. Krajewski, R. Tymkiewicz, J. Litniewski, B. Gambin, Magnetic and ultrasonic thermal effects of magnetic nanoparticles in a tissue phantom, in: 2019 Applications of Electromagnetics in Modern Engineering and Medicine (PTZE), 2019, pp. 89–92.
[13] M. Häring, J. Schiller, J. Mayr, S. Grijalvo, R. Eritja, D.D. Díaz, Magnetic gel composites for hyperthermia cancer therapy, Gels 1 (2) (2015) 135–161, https://doi.org/10.3390/gels1020135.
[14] F.A. Blyakhman, E.B. Makarova, F.A. Fadeyev, D.V. Lugovets, A.P. Safronov, P.A. Shabadrov, T.F. Shklyar, G.Y. Melnikov, I. Orue, G.V. Kurlyandskaya, The contribution of magnetic nanoparticles to ferrogel biophysical properties, Nanomaterials 9 (2) (2019), https://doi.org/10.3390/nano9020232.
[15] S. Wu, W. Hu, Q. Ze, M. Sitti, R. Zhao, Multifunctional magnetic soft composites: a review, Multifunct. Mater. 3 (4) (2020) 042003, https://doi.org/10.1088/2399-7532/abcb0c.
[16] E.C.G. Frachini, D.F.S. Petri, Magneto-responsive hydrogels: preparation, characterization, biotechnological and environmental applications, J. Braz. Chem. Soc. 10 (2019), https://doi.org/10.21577/0103-5053.20190074l0.6084.
[17] F.A. Blyakhman, S.Y. Sokolov, A.P. Safronov, O.A. Dinislamova, T.F. Shklyar, A.Y. Zubarev, G.V. Kurlyandskaya, Ferrogels ultrasonography for biomedical applications, Sensors 19 (18) (2019), https://doi.org/10.3390/s19183959.
[18] Y. Hadadian, J.H. Uliana, A.A.O. Carneiro, T.Z. Pavan, A novel theranostic platform: integration of magnetomotive and thermal ultrasound imaging with magnetic hyperthermia, IEEE Trans. Biomed. Eng. 68 (1) (2021) 68–77, https://doi.org/10.1109/TBME.2020.2990873.
[19] K.P. Kubelick, M. Mehrmohammadi, Magnetic particles in motion: magneto-motive imaging and sensing, Theranostics 12 (2020) 1783–1799, https://doi.org/10.7150/thno.54056.
[20] B. Gambin, E. Kruglenko, Ultrasonic specific absorption rate in nanoparticle-mediated moderate hyperthermia, Bull. Pol. Acad. Sci., Tech. Sci. 69 (3) (2021) e137053, http://journals.pan.pl/Content/119619/PDF/Bpast.No.69(3)310187324.06.21Druk.pdf.
[21] B. Gambin, P. Melnikova, E. Kruglenko, R. Strzałkowski, M. Krajewski, Impact of the agarose ferrogel fine structure on magnetic heating efficiency, J. Magn. Magn. Mater. 550 (2022) 169000, https://doi.org/10.1016/j.jmmm.2021.169000.
[22] B. Gambin, P. Melnikova, E. Kruglenko, R. Strzałkowski, M. Krajewski, Corrigendum to “impact of the agarose ferrogel fine structure on magnetic heating efficiency”, J. Magn. Magn. Mater. 550 (2022) 169000, https://doi.org/10.1016/j.jmmm.2022.169423, J. Magn. Magn. Mater. 556 (2022) 169423.
[23] M. Zahn, Electromagnetic Field Theory: A Problem Solving Approach, Wiley, New York, 1979.
[24] A. Skumiel, K. Kaczmarek, D. Flak, M. Rajnak, I. Antal, H. Brząkała, The influence of magnetic nanoparticle concentration with dextran polymers in agar gel on heating efficiency in magnetic hyperthermia, J. Mol. Liq. 304 (2020) 112734, https://doi.org/10.1016/j.molliq.2020.112734.
[25] A. Włodarczyk, S. Gorgoń, A. Radon, K. Bajdak-Rusinek, Magnetite nanoparticles in magnetic hyperthermia and cancer therapies: challenges and perspectives, Nanomaterials 12 (2022) 1807, https://doi.org/10.3390/nano12111807.
[26] P. Ilg, M. Kröger, Field-and concentration-dependent relaxation of magnetic nanoparticles and optimality conditions for magnetic fluid hyperthermia, Sci. Rep. 12 (2023) 116523, https://doi.org/10.1038/s41598-023-43140-8.
[27] H. Fatima, T. Charinpanitkul, K.-S. Kim, Fundamentals to Apply Magnetic Nanoparticles for Hyperthermia Therapy, Nanomaterials, Basel, Switzerland, 2021, p. 20210501.
[28] B. Karaböce, K. Kılıç, G. Erdoğan, Investigation of ultrasonic fields produced by hifu transducers used in cancer therapy, in: 2016 IEEE International Symposium on Medical Measurements and Applications (MeMeA), 2016, pp. 1–4.
[29] R. Hergt, S. Dutz, Magnetic particle hyperthermia—biophysical limitations of a visionary tumour therapy, J. Magn. Magn. Mater. 311 (1) (2007) 187–192, https://doi.org/10.1016/j.jmmm.2006.10.1156, Proceedings of the Sixth International Conference on the Scientific and Clinical Applications of Magnetic Carriers.
[30] R. Rosensweig, Heating magnetic fluid with alternating magnetic field, J. Magn. Magn. Mater. 252 (2002) 370–374, https://doi.org/10.1016/S0304-8853(02)00706-0, Proceedings of the 9th International Conference on Magnetic Fluids.
[31] M. Lévy, F. Gazeau, J.-C. Bacri, C. Wilhelm, M. Devaud, Modeling magnetic nanoparticle dipole-dipole interactions inside living cells, Phys. Rev. B 84 (2011) 075480, https://doi.org/10.1103/PhysRevB.84.075480.